RSC Advances

ROYAL SOCIETY OF CHEMISTRY

www.rsc.org/advances

Cite this: DOI: 10.1039/c0xx00000x

www.rsc.org/xxxxxx

PAPER

Inorganic-organic hybrid NiO-g-C_3N_4 photocatalyst for efficient methylene blue degradation using visible light

Hai-Yu Chen,[a, b] Ling-Guang Qiu,[a,] *Juan-Ding Xiao,[a] Sheng Ye,[a] Xia Jiang,[a] Yu-Peng Yuan,[a, b,] *

Received (in XXX, XXX) Xth XXXXXXXXX 20XX, Accepted Xth XXXXXXXXX 20XX

DOI: 10.1039/b000000x

Inorganic-organic hybrid NiO-g-C_3N_4 photocatalysts with different NiO contents were prepared through a simple calcination method. The asprepared photocatalysts were characterized by powder X-ray diffraction (PXRD), thermo-gravimetric analysis (TGA), Brunauer-Emmett-Teller (BET) method, high-resolution transmission electron microscopy (HR-TEM), and UV-vis diffuse reflection spectroscopy (UV-vis). The photocatalytic degradation of Methylene Blue (MB) over NiO-g-C_3N_4 was investigated. The incorporation of NiO caused a red-shift of the UV-vis absorption edge of g-C_3N_4. And the NiO-g-C_3N_4 photocatalysts exhibited a significantly enhanced photocatalytic activity in degrading MB using visible light, and the optimum hybrid photocatalyst with 6.3 wt. % NiO showed a 2.3 times enhanced MB degradation rate. The improved photoactivity of NiO-g-C_3N_4 photocatalysts could be ascribed to the effective interfacial charge transfer between NiO and g-C_3N_4, thus suppressing the recombination of the photoexcited electron-hole pairs. Furthermore, the NiO-g-C_3N_4 photocatalyst showed excellent stability for the photocatalytic degradation of MB.

Introduction

Photocatalysis is a catalytic process on the surface of semiconductor materials with the irradiation of photons.[1] Up to now, a large number of semiconductor materials, such as metal oxides, metal sulfides, mixed oxide (ZnO, NiO, CdS, NiO/TiO_2) have been used as active photocatalysts for organic pollutants photodegradation.[2] However, most of the developed photocatalysts containing metals can only work in the ultraviolet region with moderate performance.

Polymeric graphitic carbon nitride (g-C_3N_4) has received tremendous attentions due to its excellent photocatalytic splitting water and degradation of organic pollutants under visible light irradiation.[3-5] This polymeric semiconductor is a "sustainable" photocatalyst as it only contains C and N element. However, the photoactivity of g-C_3N_4 is relatively lower compared with several inorganic photocatalysts, such as Ag_3PO_4 and Ag/AgCl.[6] For improving the photoactivity of g-C_3N_4, a lot of attempts have been made.[7] For example, Zhang et al.[6a] reported that g-C_3N_4 could be reversibly protonated by strong mineral acids, so as to modify its solubility, dispersability, electronic structure and increase its surface area. Another feasible strategy for improving its photoactivity is to couple g-C_3N_4[8] with other inorganic semiconductors to form heterostructure as this heterostructure can improve the charge separation and enhance the photoactivity.[9] Wang *et al.*[10] demonstrated that the UV photoactivity of MB degradation was improved about 3.5 times by coupling ZnO with g-C_3N_4. Very recently, Li *et al.*[11] reported that $SmVO_4$ photocatalyst hybridized with g-C_3N_4 can improve the photodegradation efficiency of Rhodamine B (RhB). These results confirm that coupling g-C_3N_4 with energy position matched semiconductors could evidently enhance the photocatalytic acitivity of g-C_3N_4.

Herein, we synthesized a new inorganic-organic hybrid NiO-g-C_3N_4 photo-catalyst by calcining the melamine and nickel acetate precursors. It was found that the incorporation of NiO enhanced the visible light absorption of g-C_3N_4, and the photodegradation activity of NiO-g-C_3N_4 for MB was greatly enhanced under visible light irradiation comparing with the pristine g-C_3N_4. And the resultant hybrids show excellent stability during the photochemical reactions. The mechanism for this enhanced photocatalytic MB degradation can be ascribed to the interfacial charge transfer between NiO and g-C_3N_4 based on the photoluminescence results.

Experimental Section

Melamine and nickel acetate tetrahydrate were purchased from Sinopharm (Shanghai) Chemical Reagent Co., Ltd. All other reagents are of analytically pure and used as received without further purification.

Photocatalyst Preparation

In a typical synthesis, a desired amount of nickel acetate tetrahydrate (0.016, 0.035, 0.048, 0.065, 0.075 and 0.085g for sample **1**, **2**, **3**, **4**, **5**, and **6**, respectively) was fristly dissolved in 2 mL of ethanol, and then melamine (2.0 g, 15.8 mmol) was added and dispersed by ultrasonic for 5 min. The mixtures were dried at 85 ^oC overnight to remove ethanol. Subsequently, the as prepared mixtures were put into a crucible with cover and heated to 500 ^oC for 2 h with a heating rate of 20 ^oC min^{-1} and 520 ^oC for another 2 h in a muffle furnace (see Fig. 1). The pristine g-C_3N_4 was also

prepared for comparison purpose.

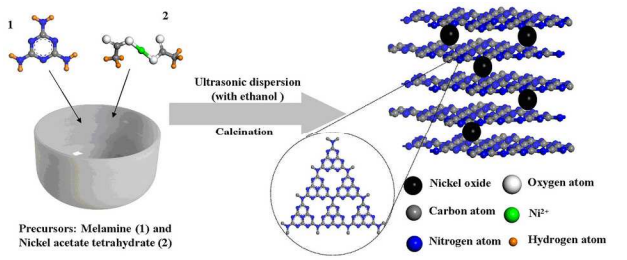

Fig. 1 A schematic illustration of synthetic process of the NiO-g-C_3N_4 photocatalysts.

Photocatalyst characterizations

PXRD patterns of the as prepared samples were collected on Philips-1700X diffractometer (Cu-Kα_1 radiation, λ=1.54056 Å) using a step scan model from 5 °~70 °. TGA was carried out from room temperature to 800 °C under air atmosphere, using a Pyris1 TGA-1 analyzer. The microstructures of the NiO-g-C_3N_4 hybrid catalysts were observed by high-resolution transmission electron microscopy on a JEOLJEM 2100 transmission electron microscope at 200 kV. The Brunauer-Emmett-Teller surface areas of as prepared samples were analyzed over a ASAP-2020 analyzer at 77 K. The UV-vis diffuse reflectance spectrum was collected at room temperature over the spectral range 200~800 nm on Shimadzu UV-3900 spectrophotometer, using $BaSO_4$ as a reference. Fluorescence spectra were obtained at an excitation wavelength of 298 nm using a Hitachi F-4500 fluorescence spectrophotometer at room temperature.

Photocatalytic Activity Tests

In order to test the photocatalytic activities of the asprepared NiO-g-C_3N_4 hybrid catalysts, MB was chosen as the target pollutant. Visible light was produced by a light irradiation system containing a Xe-lamp (XQ-500W, Shanghai, China) with a 420 nm cut-off optical filter. In a typical photocatalytic experiment, 0.050 g of catalyst was dispersed in MB aqueous solution (100 mL, 5 mg L^{-1}). The suspension was first magnetically stirred in dark for 1 h to establish the adsorption-desorption equilibrium (see Fig. S1, MB concentration kepts constant after 40 min adsorption over the catatalysts), then 0.1 mL H_2O_2 was added as an electron acceptor to suppress the electron-hole pair recombination[12]. The MB concentration change was monitored by measuring the absorption at λ = 664 nm using a UV-visible spectrophotometer (UV-3900, Shimadzu). The values of experimental results were used to draw the plot. The repeated usages of NiO-g-C_3N_4 **3** for MB degradation were carried out under the same conditions.

Results and discussion

Characterization of the NiO-g-C_3N_4 hybrid catalysts

The crystalline nature and composition of the as-synthesized products were first characterized by PXRD. As shown in Fig. 2, the peak at 27.4° corresponds to the characteristic interlayer stacking peak of aromatic systems in accordance with miller indices (002) (JCPDS 87-1526), while the peak at 13.1° is the characteristic peak of in-plane structural packing corresponding to miller indices (100) (JCPDS 87-1526). No peaks of NiO were observed due to its low contents in hybrid catalysts and g-C_3N_4 wrapping (see Fig. S2). In addition, no other impurity phases are detected. Besides, the crystallinity of the hybrid catalysts is similar to pristine g-C_3N_4 with an exception of sample **6**, in which the diffraction intensity is slightly decreased. This phenominon should be caused by the increased NiO contents, thus reducing the crystallinity of g-C_3N_4.

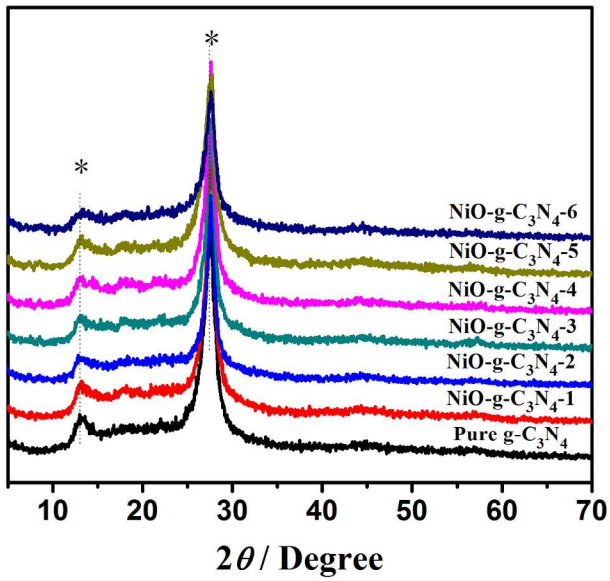

Fig. 2 PXRD patterns of g-C_3N_4 and NiO-g-C_3N_4 photo-catalysts **1**~**6**, characteristic peaks of g-C_3N_4 are marked by *.

TGA was performed to determine the NiO contents in the final hybrid catalysts. TGA analysis was performed from room temperature to 825 °C at a heating rate of 20 °C min^{-1}, as shown in Fig. 3. The g-C_3N_4 phase in the as prepared hybrid catalysts (except sample **6**) becomes unstable when the temperature is over 500 °C. This may be attributed to the excess NiO species reduced the crystallinity of g-C_3N_4. An obvious weight losses at the temperature of 520 to 660 °C reveals the combustion of g-C_3N_4. Furthermore, the NiO mass content in the hybrid catalysts could be calculated to be 2.0, 4.1, 6.3, 8.6, 9.4 and 10.1 wt. % for samples **1**~**6** after heating the samples over 700 °C, which is roughly consistent with the feeded $Ni(AC)_2{\cdot}4H_2O$ content.

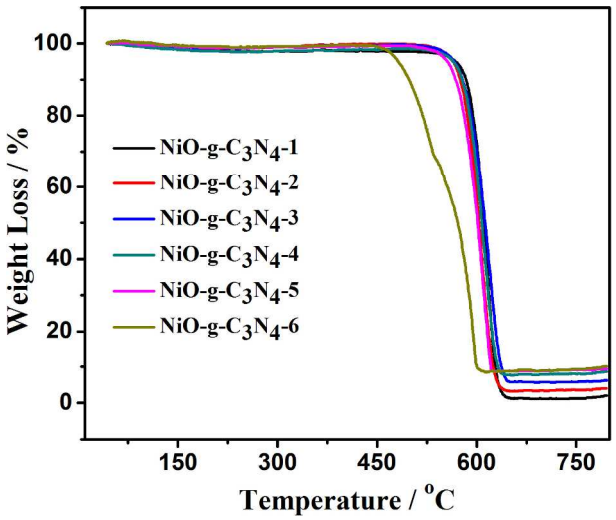

Fig. 3 TGA of the NiO-g-C_3N_4 photocatalysts **1**~**6** under air atmosphere from room temperature to 825 ºC at a heating rate of 20 ºC min^{-1}.

N_2 sorpion-desorption isotherms were performed to determine the BET surface areas of pristine g-C_3N_4 and the NiO-g-C_3N_4 hybrid catalyst. The BET values of sample **1**, **2**, **3**, **4**, **5,** and **6** were measured to be 18, 13, 34, 41, 19, 32 and 53 m^2 g^{-1} and the pore volume were 0.004, 0.002, 0.005, 0.001, 0.004, 0.001, and 0.002 cm^3 g^{-1}(corresponding pore-size distribution of sample **1**~**6**, as shown in Fig. S3). No consistency between the BET value and the NiO contents is observed. And the change in the specific surface area does not match that in the catalyst activity, for example, the catalyst **3** (41 m^2 g^{-1}) is much more efficient than catalyst **1** and **6** (13 m^2 g^{-1} and 53 m^2 g^{-1}, respectively) in photocatalytic degradation of MB (as shown in Fig. 6). Therefore, the specific BET surface area isn't the most important factor on catalytic activity. The ratio of inorganics and organics matters the most.

The existence of NiO in the hybrid photocatalysts was visulized by the TEM observations, as shown in Fig. 4. g-C_3N_4 in the hybrid catalysts shows two-dimensional (2D) lamellar structure (Fig. 4), which is consistent with results reported previously.[13] NiO nanoparticles with average size of about 10 nm were well-dispersed in the g-C_3N_4 phase (Fig. 4 c-d). The HRTEM reveals that the fringe spacing of 0.336 nm can be indexed to the (002) crystal planes of g-C_3N_4 (Fig. 4e), while the lattice spacing of 0.210 nm can be assigned to the (200) facets of NiO. More importantly, a intimate contact between NiO and g-C_3N_4 was formed (Fig. 4f), which is very important for effective interfacial charge transfer.

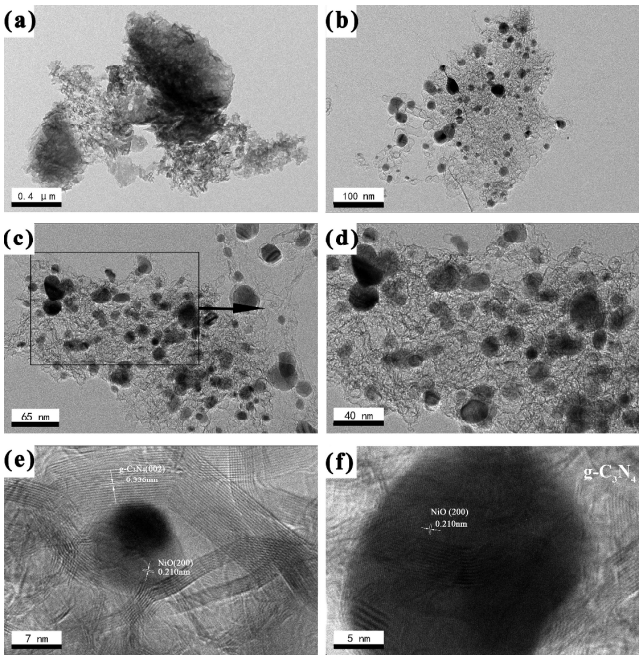

Fig. 4 TEM images (a-d) and HR-TEM images (e, f) of the cross-sectional NiO-g-C_3N_4 hybrid catalyst.

Fig. 5 shows the optical obsorption behaviors of the asprepared NiO-g-C_3N_4 catalysts and the pristine g-C_3N_4. The band gap of the hybrid catalysts were also estimated according to the formula

$$(Ahv)^{1/2} = C(hv - E_g) \quad (1)$$

Wherein A is the light absorption coefficient, h is planck's constant, v is light frequency, C is a constant, and E_g is the band gap energies.[14] The intercept to x-axis of the tangents is the band gap energies of the hybrid catalysts, as shown in the inset of Fig. 5. The band gap absorption edge of pristine g-C_3N_4 is around 450 nm (Fig. 5), corresponding to a band gap energy (E_g) of 2.7 eV, which is in agreement with the value reported in the literatures.[15]. It is noteworthy that the NiO-g-C_3N_4 hybrid catalysts show more intense absorption compared with pristine g-C_3N_4. The band-gap energy of the hybrid catalysts tends to be smaller than that of the pristine g-C_3N_4, indicating that the absorption of the NiO-g-C_3N_4 photocatalysts is shifted to the lower energy region.

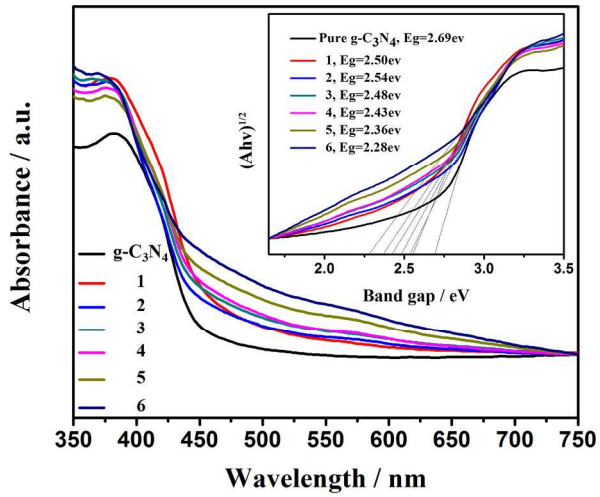

Fig. 5 UV-vis absorption spectra of pristine g-C_3N_4 and NiO-g-C_3N_4

photocatalysts **1**~**6**. Inset shows the relation of $(Ah\nu)^{1/2}$ vs. photon energy.

Photocatalytic degradation performance of the NiO-g-C_3N_4 photocatalysts

The photocatalytic degradation of MB over the NiO-g-C_3N_4 hybrid catalysts was illustrated in Fig. 6. It can be found that the MB adsorption equilibrium over NiO-g-C_3N_4 hybrids and pristine g-C_3N_4 can be reached after 60 min stirring in the dark, and the absorbed MB does not affected evidently by the NiO contents (see Fig. S1). Control experiments illustrates that no catalysts and H_2O_2 addition or H_2O_2 addition only caused 13% % and 58% MB degradation after 80 min visible light irradiation. ~ 90% of MB was degradated over prestine g-C_3N_4 after 75 min visible light irradiation. The introduction of NiO can evidently enhance the photocatalytic activity of g-C_3N_4 for MB degradation. In addition, the photocatalytic activity for MB degradation inreased gradually with the increased NiO contents. And the highest photocatalytic activity for MB degradation was occurred over sample **3**, in which the MB degradation can be completed within 40 min visible light irradiation. In comparison, a simple mixture of NiO with g-C_3N_4 only showed a similar MB degradation rate with that of pristine g-C_3N_4 (Fig. S4). These results confirm that the NiO-g-C_3N_4 hybrid photocatalysts possess superior photocatalytic capability in comparison with the pristine g-C_3N_4. Further increasing the NiO amount caused a decreased MB degradation rate. For example, the MB degradation over sample **6** can only be completed after 70 min visible light irradiation, indicating that the over-loaded NiO (8.6, 9.4 and 10.1 wt. %) had a negative effect on MB degradation. This result should be ascribed to the fact that the excessive loaded NiO may act as a recombination centre and cover the active sites on the g-C_3N_4 surface, thus decreasing the efficiency of charge separation[16]. These results show that there is an optimum NiO loading amount upon g-C_3N_4 for efficient photocatalyzed degradation of MB under visible light irradiation.

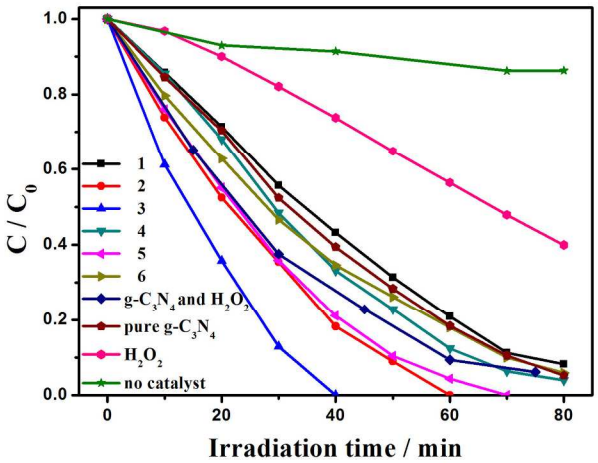

Fig. 6 Photocatalytic properties of pristine g-C_3N_4 and NiO-g-C_3N_4 photocatalysts **1** ~ **6**.

To further understand the reaction kinetics of MB degradation over NiO-g-C_3N_4 hybrids, the experimental data were fitted by first-order kinetics reaction equation model, as expressed by equation 2. Table 1 summarizes the fitted kinetic results.

$$-\ln(C/C_0) = kt \quad (2)$$

where k is the rate constant (min^{-1}), C_0 and C are the MB concentration of initial and at time t, respectively. As shown in Table 1, all linear correlation coefficients (R) approach to 1, demonstrating that all data fit the first-order kinetics reaction equation model well. Fig .7a shows a linear relationship between $\ln(C/C_0)$ and the irradiation time for MB degradation catalyzed over prestine g-C_3N_4, and NiO-g-C_3N_4 hybrid **2** and **3**. All plots of $\ln(C/C_0)$ against the irradiation time (t) are linear. The rate constant (k (min^{-1})) of pristine g-C_3N_4 (0.0218 min^{-1}) is constent with the previously reported value.[17] The kinetic constants of NiO-g-C_3N_4 photocatalysts **1**~**6** are larger than that of g-C_3N_4 (Fig. 7b). And the largest kinetic constant of sample **3** (0.0510 min^{-1}) is 2.3 times higher than that of pristine g-C_3N_4 (0.0218 min^{-1}) under the same experimental conditions. This result demonstrates that the introduction of NiO could efficiently enhance the photocatalytic activity of g-C_3N_4 under visible light irradiation.

Table 1 Summary of linear correlation coefficients(R), rate constant (k(min^{-1})) and the standard error of linear fitting.

Sample	R	k(min^{-1})	Standard error (±)
g-C_3N_4	0.989	0.022	0.001
1	0.976	0.027	0.001
2	0.998	0.034	7.98E-4
3	0.999	0.051	6.74E-4
4	0.967	0.033	0.002
5	0.987	0.036	0.002
6	0.991	0.029	9.39E-4

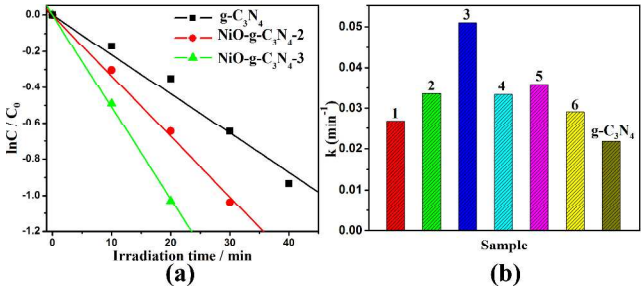

Fig. 7 (a) First-order kinetics plot, and (b) the photodegradation of MB under visible light irradiation (λ > 420 nm) by g-C_3N_4, NiO-g-C_3N_4 photocatalysts **1**~**6**.

Considering the practical applications, the long-term photostability is very important. Fig. 8 shows the 5 consecutive usages of sample **3** for MB degradation under visible light irradiation. In each test, the photocatalyst was reused after centrifuged, washed with ethanol and dried at 70 °C while other factors were kept identical. No obvious loss of the photocatalytic activity of NiO-g-C_3N_4 for MB degradation was observed after five repeated usages (The MB degradation efficiency decreases ~ 2.0% after five consecutive usages). Furthermore, No changes in PXRD patterns of the NiO-g-C_3N_4 before and after five circular reactions were observed, clearly suggesting the long-term stability of the as prepared NiO-g-C_3N_4 hybrids.

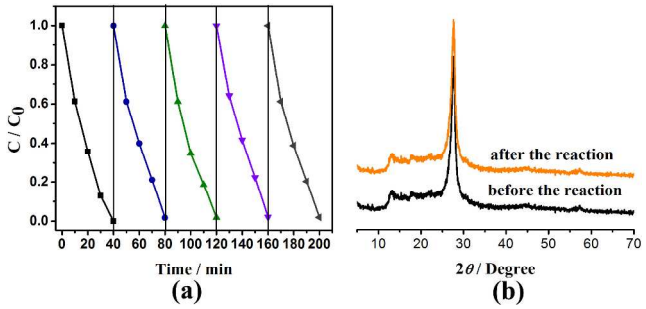

Fig. 8 (a) The photocatalytic MB degradation during five consecutive runs over sample **3** with the H_2O_2 electron acceptor; (b) PXRD patterns of the sample **3** before and after circular reactions.

Enhancement Mechanism of Photocatalytic Activity

The photoluminescence (PL) spectra were measured to monitor the electron transfer in NiO-g-C_3N_4 hybrids. For photo-luminescence measurement, a trial excitation wavelength (λ_{Ex1}) was used to record the fluorescent spectrum, in which the emission wavelength (λ_{Em1}) can be obtained at its most intensive peak. Then this measured λ_{Em1} was used to scan the excitation spectrum, and λ_{Ex2} getted. The true excitation wavelength can be determined when the $\lambda_{Ex2}=\lambda_{Ex1}$. In our experiments, an excitation wavelength of 298 nm was determined to measure the emission spectra of NiO-g-C_3N_4 hybrids. As shown in Fig. 9, the pristine g-C_3N_4 displayed a strong emmission peak at 437 nm. Notably, an significant decreased PL intensity was occurred in the NiO-g-C_3N_4 hybrid photocatalyst. Since the CB edge of g-C_3N_4 (-1.12 eV vs. NHE[11]) is more negative than that of NiO (-0.5 V vs. NHE[18]), the photoexcited electrons on g-C_3N_4 surface could inject into the NiO *via* the well developed interface[19], as shown in Fig. 4f. Similarly, the photoinduced holes on the NiO surface could move towards the g-C_3N_4 due to the difference in valence band (VB) edge potentials. Thus this decreased PL intensity might be caused by the effective interfacial charge transfer between NiO and g-C_3N_4 across the interface. As reported previously, the excited electrons could be captured by H_2O_2 to generating the hydroxyl radical (•OH).[20] The formed •OH could readily oxidize the pre-absorbed MB molecules upon the surface of the photocatalyst. Meanwhile, the photoexcited holes also can directly oxidize the MB molecules[21]. Therefore, the enhanced photocatalytic MB degradation could be caused by the effective interfacial charge transfer between NiO and g-C_3N_4, as schematically illustrated in Fig. 10.

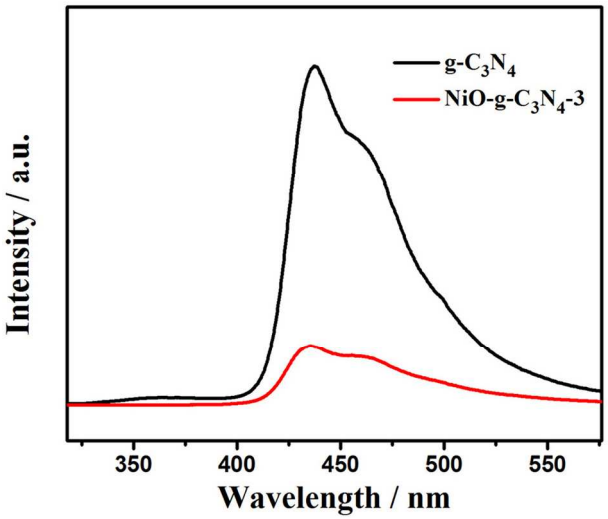

Fig. 9 Photoluminescence spectra of g-C_3N_4 and sample **3** (6.3 wt. % NiO).

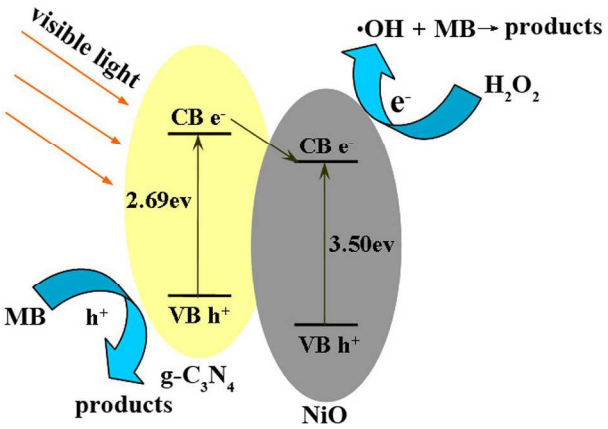

Fig. 10 Schematic illustration for the conceivable mechanism of MB photodegradation over NiO-g-C_3N_4.

Conclusions

The hybrid NiO-g-C_3N_4 photocatalysts were facilely synthesized by a calcination process. Significantly, the introduction of NiO can evidently enhance the photocatalytic activity of g-C_3N_4. And the optimum hybrid photocatalyst with 6.3 wt. % NiO loading shows a 2.3 times higher MB degradation rate than that of the pristine g-C_3N_4. Such a remarkably enhanced photocatalytic performance can mainly be attributed to the effective interfacial charge transfer between NiO and g-C_3N_4, thus suppressing the recombination of the photoexcited electron-hole pairs. The present work demonstrates a new strategy for designing recyclable g-C_3N_4 hybrid photocatalysts with high photocatalytic performance under visible light.

Acknowledgments

This work was finacially supported by the National Natural Science Foundation of China (20371002), Anhui Provincial Natural Science Foundation (1408085MB22), and the National "211 Project" of Anhui University.

Notes and references

a Laboratory of Advanced Porous Materials, School of Chemistry and Chemical Engineering, Anhui University, Hefei, China. Fax: +86 551 65108212; Tel: +86 551 65108212; E-mail: yupengyuan@ahu.edu.cn; lgqiu@ahu.edu.cn

b Innovation Lab for Clean Energy & Green Catalysis, Anhui University, Hefei 230601, P. R. China

1 (a) P. V. Kamat, Chem. Rev., 1993, 93, 267; (b) M. R. Hoffmann, S. T. Martin, W. Y. Choi, D. W. Bahneann, Chem. Rev., 1995, 95, 69; (c) A. Fujishima, K. Honda, Nature, 1972, 238, 37-38; (d) A. L. Linsebigler, G. Q. Lu, J. T. Yates, Chem. Rev., 1995, 95, 735; (e) A. Hagfeldt, M. Gratzel, Chem. Rev., 1995, 95, 49; (f) E. M Rodriguez, G. Márquez, E. A. León, P. M. Álvarez, A. M. Amat, F. J. Beltrán, J. Environ. Manage., 2013, 127, 114; (g) W. J. Wang, L. Z. Zhang, T. C. An, G. Y. Li, H. Y. Yip, P. K. Wong, Appl. Catal. B: Environ., 2011, 108, 108.

2 (a) J. L. Yang, S. J. An, W. I. Park, G. C. Yi, W. Choi, Adv. Mater., 2004, 16, 1661; (b) G. S. Pozan, M. I. Isleyen, Gokcen, Sinem, Appl. Catal. B: Environ., 2013, 140, 537; (c) F. S. Tian, Y. L. Liu, Scripta Mater., 2013, 69, 417; (d) X. Wan, M. Yuan, S. L. Tie, Appl. Surf. Sci., 2013, 177, 40; (e) L. P. Xu, Y.L. Hu, C. Pelligra, C. H. Chen, L. Jin, H. Huang, S. Sithambaram, M. Aindow, R. Joesten and S. L. Suib, Chem. Mater., 2009, 21, 2875; (f) X. L. Xing, R.J. Lu, Z. L. Wang, B. Z. Ren, Z. X. Jiang, H. Zhao, H. B. Cao, G. J. Zhang, T. Zhang, J. Nanosci. Nanotechnol., 2013, 13, 4616; (g) N. Zhang, M. Q. Yang, Z. R. Tang, Y. J. Xu, J. Catal., 2013, 303, 60.

3 X. C. Wang, K. Maeda, A. Thomas, K. Takanabe, G. Xin, J. M. Carlsson, K. Domen, M. Antonietti, Nat. Mater., 2009, 8, 76.

4 G. Liu, P. Niu, C. H. Sun, S. C. Smith, Z. G. Chen, G. Q. Lu, H. M. Cheng, J. Am. Chem. Soc., 2010, 132, 11642.

5 (a) Y. Zheng, J. Liu, J. Liang, M. Jaroniecc, S. Z. Qiao, Energy Environ. Sci., 2012, 5, 6717; (b) F. Dong, L. W. Wu, Y. J. Sun, M. Fu, Z. B. Wu, S. C. Lee, J. Mater. Chem., 2011, 21, 15171; (c) J. H. Liu, T. K. Zhang, Z. C. Wang, G. Dawson, W. Chen, J. Mater. Chem., 2011, 21, 14398.

6 (a) Y. J. Zhang, A. Thomas, M. Antonietti, X. C. Wang, J. Am. Chem. Soc., 2009, 131, 50; (b) Y. Liu, G. Chen, C. Zhou, Y. D. Hu, D. G. Fu, J. Liu, Q. Wang, J. Hazard. Mater., 2011, 190, 75; (c) S. C. Yan, S. B. Lv, Z. S. Li, Z. G. Zou, Dalton Trans., 2010, 39, 1488; (d) G. Liu, P. Niu, C. H. Sun, S. C. Smith, Z. G. Chen, G. Q. Lu, H. M. Cheng, J. Am. Chem. Soc., 2010, 132, 11642.

7 (a) L. Y. Huang, H. Xu, Y. P. Li, H. M. Li, X. N. Cheng, J. X. Xia, Y. G. Xu, G. B. Cai, Dalton Trans., 2013, 42, 8606; (b) K. Katsumata, R. Motoyoshi, N. Matsushita, K. Okada, J. Hazard. Mater., 2013,260, 475; (c) F. Chang, Y. C. Xie, C. L. Li, J. Chen, J. Luo, X. F. Hu, J. W. Shen, Appl. Surf. Sci., 2013, 280, 967; (d) Y. P. Yuan, Y. W. Cao, Y. S. Liao, L. S. Yin, C. Xue, Appl. Catal. B: Environ., 2013, 140, 164; (e) L. Ge, C. C. Han, X. L. Xiao, L. L. Guo, Int. J. Hydrogen Energy, 2013, 38, 6960; (f) J. G. Yu, S. H. Wang, B. Cheng, Z. Lin, F. Huang, Catal. Sci. Technol., 2013, 3, 1782.

8 J. Fu, Y. Tian, B. Chang, F. Xi, X. Dong, J. Mater. Chem., 2012, 22, 21159.

9 (a) J. X. Sun, Y. P. Yuan, L. G. Qiu, X. Jiang, A. J. Xie, Y. H. Shen, J. F. Zhu, Dalton Trans., 2012, 41, 6756; (b) S. C. Yan, S. B. Lv, Z. S. Li and Z. G. Zou, Dalton Trans., 2010, 39, 1488; (c) X. X. Xu, G. Liu, C. Randorn and J. T. S. Irvine, J. Hydrogen Energy, 2011, 36, 13501; (d) Y. J. Wang, R. Shi, J. Lin, Y. F. Zhu, Energy Environ. Sci., 2011, 4, 2922; (e) C. S. Pan, J. Xu, Y. J. Wang, D. Li, Y. F. Zhu, Adv. Funct. Mater., 2012, 22, 1518; (f) L. Ge, C. C. Han and J. Liu, Appl. Catal. B: Environ., 2011, 108, 100; (g) H. J. Yan, H. X. Yang, J. Alloys Compd., 2011, 509, L26.

10 Y. J. Wang, R. Shi, J. Lin and Y. F. Zhu, Energy Environ. Sci., 2011, 4, 2922.

11 T. T. Li, L. H. Zhao, Y. M. He, J. Cai, M. F. Luo, J. J. Lin, Appl. Catal. B: Environ., 2013, 129, 255.

12 J. J. Du, Y. P. Yuan, J. X. Sun, F. M. Peng, X. Jiang, L. G. Qiu, A. J. Xie, Y. H. Shen, J. F. Zhu, J. Hazard. Mater., 2011, 190, 945.

13 G. Z. Liao, S. Chen, X. Quan, H. T. Yu and H. M. Zhao, J. Mater. Chem., 2012, 22, 2721.

14 M. H. M. Zaid, A. M. Khamirul, S. Hj. A. Aziz, A. Zakaria and M. S. M. Ghazali, Int. J. Mol. Sci., 2012, 13, 7550.

15 (a) X. C. Wang, K. Maeda, A. Thomas, K. Takanabe, G. Xin, J. M. Carlsson, K. Domen and M. Antonietti, Nat. Mater., 2009, 8, 76; (b) G. C. Liu, Z. Jin, X. W. Zhang, X. F. Li, H. Liu, J. Nonferrous Met., 2013, 3, 793.

16 S. Ye, L. G. Qiu, Y. Yuan,Y. J. Zhu, J. Xia and J. F. Zhu, J. Mater. Chem. A, 2013, **1**, 3008.

17 T. Muhammad, C. B. Cao, F. K. Butt, S. Butt, F. Idrees, Z. Ali, I. Aslam, M. Tanveer, A. Mahmood, N. Mahood, CrystEngComm, 2014, 16, 1825.

18 X. Yong and Martin A.A. Schoonen, American Mineralogist, 2000, 85, 543.

19 B. Chai, T. Y. Peng, J. Mao,L. Kan, Z. Ling, Phys. Chem. Chem. Phys., 2012, 14, 16745.

20 C. F. Zhang, L. G. Qiu, F. K., Y. J. Zhu, Y. P. Yuan, G. S. Xu and X. Jiang, J. Mater. Chem. A, 2013, 1, 14329.

21 A. Mills, J. S. W., J. Photochem. Photobiol. A: Chem., 1999,127, 123.

Graphical Abstract

Inorganic-organic hybrid NiO-g-C_3N_4 photocatalyst was synthesized by facile calcination. Visible-light-induced photocatalytic activity of the hybrid photocatalyst was significantly enhanced, which is due to the effective interfacial charge transfer suppressed the recombination of the photo-excited electron-hole pairs. Besides, excellent photostability for photocatalytic reaction under visible-light irradiation was detected.